ELSEVIER

Journal of Contaminant Hydrology 50 (1998) 243–264

JOURNAL OF
Contaminant
Hydrology

A numerical model for transient-hysteretic flow and solute transport in unsaturated porous media

Robert J. Mitchell [a,1], Alex S. Mayer [b,*]

[a] *Department of Geology, Western Washington University, Bellingham, WA, USA*
[b] *Department of Geological Engineering and Sciences, Michigan Technological University, 1400 Townsend Drive, Houghton, MI 49931, USA*

Received 23 September 1996; revised 17 April 1997; accepted 17 April 1997

Abstract

A two-dimensional flow and transport model was developed for simulating transient water flow and nonreactive solute transport in heterogeneous, unsaturated porous media containing air and water. The model is composed of a unique combination of robust and accurate numerical algorithms for solving the Richards', Darcy flux, and advection–dispersion equations. The mixed form of Richards' equation is solved using a finite-element formulation and a modified Picard iteration scheme. Mass lumping is employed to improve solution convergence and stability behavior. The flow algorithm accounts for hysteresis in the pressure head–water content relationship. Darcy fluxes are approximated with a Galerkin and Petrov–Galerkin finite-element method developed for random heterogeneous porous media. The transport equation is solved using an Eulerian–Lagrangian method. A multi-step, fourth-order Runge–Kutta, reverse particle tracking technique and a quadratic–linear interpolation scheme are shown to be superior for determining the advective concentration. A Galerkin finite-element method is used for approximating the dispersive flux. The unsaturated flow and transport model was applied to a variety of rigorous problems and was found to produce accurate, mass-conserving solutions when compared to analytical solutions and published numerical results. © 1998 Elsevier Science B.V.

1. Introduction

The vadose zone is prone to contamination from agricultural chemicals, hydrocarbons, and many other hazardous substances and, in some cases, functions as a receptacle

* Corresponding author. Fax: +1-906-487-3371; e-mail: asmayer@mtu.edu
[1] Fax: +1-360-650-7302; e-mail: rjmitch@henson.cc.wwu.edu

PII S0169-7722(97)00042-9

for controlled waste storage and disposal. When water is applied to the soil surface, either naturally or by irrigation, it may transport chemical contaminants through the vadose zone to the underlying groundwater aquifer. Because of the vadose zone's susceptibility to contamination and its direct link to aquifers, transport phenomena in the vadose zone are of significant environmental concern. Although vadose zone contamination by nonaqueous phase liquids is an important problem, the following work focuses on systems containing air and aqueous phases only, where the contaminant is distributed in the aqueous phase and the air phase is immobile.

Mathematical models play a significant role in the analysis of the fate and transport of contaminants in the vadose zone and in the development of water and agricultural management and remediation strategies. A common approach when modeling transport in the vadose zone is to assume ideal conditions, such as uniform water content and steady-state water flow in one-dimensional (1-D) domains (e.g., van Genuchten and Wierenga, 1976; Bresler and Dagan, 1981; Jury, 1982). The ideal approach eliminates the need for the solution of the flow equation and, therefore, minimizes the amount of model input data and the computational demand. However, results generated by ideal models often do not agree with laboratory and field observations, and their utility for predicting field-scale processes is questionable (van Genuchten, 1991).

To better approximate the transport of contaminants in the vadose zone, models should consider the physical influences of transient flow as well as the natural heterogeneity and multidimensional aspects of porous median (Nielsen et al., 1986). However, maintaining numerical accuracy when modeling transient flow and transport in unsaturated, heterogeneous porous media is difficult (Gee et al., 1991). Serious mass balance and convergence problems can develop due to the nonlinear nature of the unsaturated flow equation (Richards' equation), particularly when using the pressure-head-based form (Celia and Bouloutas, 1990). Some of these problems have been resolved through the development of schemes using the mixed form of Richards' equation (Allen and Murphy, 1986; Celia et al., 1987; Celia and Bouloutas, 1990). An algorithm based on a fully-implicit time approximation and a modified Picard iteration scheme applied to the mixed-form of Richards' equation has produced accurate solutions with excellent global mass balance (Celia and Bouloutas, 1990).

Some studies have shown that hysteresis in the water content–pressure head relation can impede solute transport in the vadose zone (e.g., Russo et al., 1989). In order to model hysteresis, a family of scanning curves bounded by main wetting and draining curves is used to describe the relationship between pressure heads and water contents. Parker and Lenhard (1987) introduced a technique similar to the models of Scott et al. (1983) and Kool and Parker (1987), where scanning curves are generated by applying scaling relations to the main wetting and draining curves. The advantage of the method of Parker and Lenhard (1987) is that closure of the scanning loops is enforced to eliminate the pumping effect, which can cause mass balance errors (Jaynes, 1984).

Since the Darcy flux is the only coupling between flow and transport, it is imperative that the flux is calculated with precision. Finite-difference methods for calculating fluxes from predetermined heads are easy to apply and are efficient, but produce velocities that are discontinuous at element boundaries. These discontinuities can cause local mass balance errors, which may accumulate globally and produce errors in transport computa-

tions (Yeh, 1981). The finite-element method introduced by Yeh (1981) produces continuous velocities at element boundaries and better mass balance accuracy than finite-difference methods. A scheme based on the finite-element method of Yeh (1981) was developed for multidimensional heterogeneous porous media by Srivastava and Brusseau (1995). This method was shown to be accurate in random heterogeneous porous media where the contrast between hydraulic properties was not large.

With the mixed finite-element method, the pressure head and Darcy flux are determined simultaneously, which produces Darcy fluxes with a higher order of accuracy than the finite-difference and finite-element methods (e.g., Chiang et al., 1989). Unfortunately, the mixed method requires the most computational effort of all the methods. It has not been demonstrated that the potential increase in accuracy obtained with the mixed finite-element method is sufficient to justify the extra computational burden for transient, unsaturated problems in multiple dimensions.

There are many algorithms in the literature for the numerical solution of the advection–dispersion equation. The application of finite-element methods is subject to local Peclet and Courant number restrictions, i.e., $\mathrm{Pe} \leq 2$ and $\mathrm{Cr} \leq 1$, where the local Peclet number is defined as $\mathrm{Pe} = v\Delta l/D$, v is the pore water velocity, Δl is the characteristic length of the element, D is the dispersion coefficient, the local Courant number is defined as $\mathrm{Cr} = v\Delta t/\Delta l$, and Δt is the time step. Upstream weighting methods were developed to improve finite-element solutions by reducing numerical oscillations under high Pe conditions (Sudicky and Huyakorn, 1991). The Petrov–Galerkin, finite-element upstream weighting technique developed by Westerink and Shea (1989) and Cantekin and Westerink (1990) has been shown to produce stable, accurate solutions (Noorishad et al., 1992) for high Peclet numbers ($\mathrm{Pe} < \infty$), but it is still subject to the restriction that $\mathrm{Cr} < 1$.

Transport models based on Eulerian–Lagrangian methods, specifically the modified method of characteristics (MMOC) have been shown to be a practical alternative for advective-dominated problems in saturated porous media (e.g., Chiang et al., 1989). The MMOC method, which employs a fixed grid system, is more computationally efficient than forward particle tracking or adaptive techniques (Zhang et al., 1993) and, unlike finite-element methods, the MMOC method is not limited to the constraint that $\mathrm{Cr} < 1$. Binning and Celia (1996) introduced a finite volume, Eulerian–Lagrangian localized adjoint (ELLAM) method to solve the advective–dispersive transport equation and showed that the method was accurate over a wide range of Pe and Cr. However, the MMOC and ELLAM methods have not been extensively applied in heterogeneous or unsaturated porous media.

The objective of this study is to develop a numerical model that is capable of accurately simulating transient-hysteretic flow and solute transport in a 2-D, unsaturated, heterogeneous domain. The model is constructed from accurate, efficient, and mass conserving techniques. The model employs the mass-conserving, finite-element formulation of Celia and Bouloutas (1990) for approximating the pressure head and associated water contents. The methods of Parker and Lenhard (1987) and Lenhard and Parker (1987) are used to estimate hysteresis in the pressure-saturation relationships. The finite-element scheme of Srivastava and Brusseau (1995) is applied to estimate the Darcy flux. A variety of backtracking and interpolation techniques are investigated to

determine the most appropriate methods for applying the MMOC algorithm in 2-D, transient, unsaturated, heterogeneous conditions. The model is applied to flow and transport problems and the numerical results are compared against analytical solutions and published numerical results.

2. Governing equations

The general algorithm for the model developed in this work is to solve, in sequence, the water mass conservation equation, Darcy's flux equation, and the solute mass conservation equation, subject to initial and boundary conditions.

2.1. Flow equation

The nonlinear partial differential equation most commonly used to predict the pressure head field and associated water contents in the domain is known as Richards' equation. The application of Richards' equation assumes that the porous media is rigid, the fluid is incompressible and isothermal, the fluid density is unaffected by solute concentrations, and the air phase does not affect water flow. Also, Richards' equation does not explicitly account for preferential flow or other non-continuum flow phenomena. The mixed form of Richards' equation can be written as:

$$\frac{\partial \theta}{\partial t} = \nabla \cdot \left[K(\theta) \cdot \nabla(\psi - z) \right]. \tag{1}$$

Here, ψ is the pressure head, θ is the volumetric water content, defined as the volume of water in the void space divided by the bulk volume. The hydraulic conductivity in Eq. (1) is assumed to be isotropic and is defined as:

$$K(\theta) = \frac{\rho g \kappa k_r(\theta)}{\mu} = K_s k_r(\theta), \tag{2}$$

where ρ is the water density, g is the gravitational constant, κ is the intrinsic permeability, $k_r(\theta)$ is the relative permeability, K_s is the saturated hydraulic conductivity, and μ is the water dynamic viscosity.

For closure, constitutive relationships are necessary for the $\theta(\psi)$ and $K(\theta)$ functions. These constitutive relationships, which contribute to the nonlinearity of Eq. (1), are porous media specific and hysteretic in nature. The empirical relationships of van Genuchten (1980) and the van Genuchten (1980) and Mualem (1976) were used to describe the hydraulic constitutive relationships. These relationships were chosen because of the wider availability of parametric data and the availability of a reliable hysteresis algorithm. The relationships are expressed as:

$$S_e = \left[1 + |\alpha \psi|^n \right]^{-m}, \tag{3}$$

$$\theta(\psi) = \theta_{ir} + (\theta_s - \theta_{ir}) S_e, \tag{4}$$

$$k_r(\theta) = S_e^{1/2} \left[1 - \left(1 - S_e^{1/m} \right)^m \right]^2, \tag{5}$$

where S_e is the effective (normalized) water saturation, α, n, and m $(=1-1/n)$ are fitting parameters which describe the shape of the functions, θ_s is the saturated water content, and θ_{ir} is the irreducible water content.

Modified versions of the $\psi(\theta)$ hydraulic relationships are used when hysteresis is considered in the simulations. Hysteresis is modeled using the method of Parker and Lenhard (1987) and Lenhard and Parker (1987), which has been shown to compare well with experimental results (Lenhard et al., 1991). This approach simulates scanning curves between the main wetting and draining curves by scaling the main curves and forcing the scanning curves to pass through appropriate reversal points. An advantage of the method of Parker and Lenhard (1987) over other methods is that closure of the scanning loops is enforced, which minimizes mass balance problems. Their hysteresis algorithm also incorporates air entrapment by scaling the water permeabilities. Since hysteresis associated with $K(\theta)$ functions for wetting phases is assumed to be small (Mualem, 1976), hysteresis in the $K(\theta)$ function is ignored in this work.

2.2. Darcy flux

Darcy's law, which is coupled to Eq. (1) by $K(\theta)$ and $\theta(\psi)$, is used to determine the water flux field. Although Darcy's law was derived for saturated media, it is applied to unsaturated media. The flux equation is given as:

$$\boldsymbol{q} = \boldsymbol{v}\theta = -\left[K(\theta)\cdot\nabla(\psi - z)\right], \tag{6}$$

where $\boldsymbol{q}$ is the Darcy flux vector, $\boldsymbol{v}$ is the pore velocity vector, and z is the elevation measured positive downward.

2.3. Advection–dispersion equation

The advection–dispersion transport equation, which is coupled to Eqs. (1) and (6) by $\theta(\psi)$ and $\boldsymbol{q}$, is used to determine solute concentrations. The solute transport equation for a nonreactive substance in the water phase is given by (Bear, 1979):

$$\frac{\partial(\theta C)}{\partial t} = \nabla\cdot(\theta\boldsymbol{D}\cdot\nabla C) - \nabla\cdot(\boldsymbol{q}C), \tag{7}$$

where C is the solute concentration and $\boldsymbol{D}$ is the dispersion tensor as defined by Bear (1979):

$$\boldsymbol{D}_{ij} = \lambda_T|v|\delta_{ij} + (\lambda_L - \lambda_T)\frac{v_i v_j}{|v|} + D_d\tau\delta_{ij}, \tag{8}$$

where λ_L and λ_T are the longitudinal and transverse pore-scale dispersivities, respectively; δ_{ij} is the Kronecker delta; v_i and v_j are the ith and jth components of the average pore velocity, respectively; $|v|$ is the magnitude of the total pore velocity vector; D_d is the molecular diffusion; and τ is the tortuosity; which can be evaluated by relationships such as that of Millington and Quirk (1961), where $\tau = \theta^{7/3}/\theta_s^2$.

3. Numerical methodology

3.1. Solution of Richards' equation

The finite-element approximation described by Celia and Bouloutas (1990) was used to discretize the 2-D form of Eq. (1). A standard Galerkin finite-element method was used with bilinear shape functions to approximate the spatial derivatives. Green's formula was applied to reduce the second derivative terms to first-order derivatives and boundary terms. A first-order, fully-implicit, finite-difference method was used to approximate the temporal derivative. The temporal terms resulting from the finite-element approximation were lumped to improve solution convergence and stability behavior (Celia and Bouloutas, 1990). A modified Picard iteration method is used to linearize the equation. The discretized form of the equation is given in Appendix A. Application of these numerical methods results in the following matrix-vector equation:

$$\left[A_p\right]^{l+1,m}\left\{\psi_i\right\}^{l+1,m+1}=\left\{B_p\right\}^{l+1,m}, \tag{9}$$

where the superscripts l and m are the time and iteration levels, respectively. For 1-D problems, the matrix-vector equation is solved with a direct banded LUD solver. For 2-D problems, a biconjugate gradient squared iterative method with a Jacobi preconditioner from the NSPCG software package (Oppe et al., 1988) is applied. At each iteration level, new hydraulic coefficients are calculated using Eqs. (3)–(5).

3.2. Solution of the Darcy flux equation

A finite-element method has been developed by Yeh (1981) to approximate the Darcy fluxes (hereafter referred to as Yeh's FEM). The method produces nodal fluxes that vary linearly within an element and are continuous on the element boundaries. Yeh's FEM reduces mass balance errors that can be associated with finite-difference techniques, but requires more computational effort. Yeh's FEM was shown to be sufficiently accurate in variably saturated conditions by Yeh et al. (1993). The discretization is performed by applying the Galerkin method to Eq. (6) using bilinear shape functions. This scheme generates a set of N linear equations each for the x- and z-components of the Darcy flux. In matrix-vector notation, the equations can be written as:

$$\left[A_x\right]\left\{q_x\right\}^{l+1}=\left\{B_x\right\}^{l+1}, \tag{10}$$

$$\left[A_z\right]\left\{q_z\right\}^{l+1}=\left\{B_z\right\}^{l+1}. \tag{11}$$

The discretized form of the equations are given in Appendix A. The coefficient matrices $[A_x]$ and $[A_z]$ are time invariant and need to be inverted only once. The solution procedure decouples the two flux components such that each set of N linear simultaneous equations has to be solved for each flux component at each time step.

When considering a 2-D domain having heterogeneous porous media (or variably-saturated homogenous porous media), the flux component normal to a material boundary should be continuous, while the tangential component should, in general, have a jump discontinuity (Srivastava and Brusseau, 1995). To preserve the discontinuity in the

tangential direction, a scheme developed by Srivastava and Brusseau (1995) is applied. This scheme applies Yeh's FEM, but on a row by row and column by column basis in 2-D domains. The resulting z-components of the flux will be linear and continuous in the z-direction, but have jump discontinuities at the element boundaries in the x-direction. A similar result is obtained for the x-components of the flux. In this way, nodes will have a different flux value depending on from which direction the boundary is approached. Srivastava and Brusseau (1995) have shown that this scheme is more accurate than Yeh's FEM and comparable finite-difference methods in simulations of randomly heterogeneous porous media where the element boundaries corresponded with material interfaces.

The solution for the fluxes in the x-direction (lateral) are determined by applying Yeh's FEM one column at a time. In matrix-vector notation the equations can be written as:

$$\left[A_{L_x}\right]\{q_x\}^{l+1} = \left\{B_{L_x}\right\}^{l+1}, \tag{12}$$

where L_x defines the length of the column. The z-component of the Darcy flux is estimated on a row by row basis:

$$\left[A_{L_z}\right]\{q_z\}^{l+1} = \left\{B_{L_z}\right\}^{l+1}, \tag{13}$$

where L_z represents the length of each row. Instead of solving a set of N simultaneous equations for each direction, a series of uncoupled, symmetric, banded systems are solved, which is more efficient than solving the coupled system. The matrix-vector equations are solved with a direct banded LUD solver.

3.3. Solution of the advection–dispersion equation

The MMOC method was implemented to approximate the advection–dispersion equation, Eq. (7), because of its applicability in heterogeneous environments where Courant numbers are expected to exceed the critical value Cr = 1. Given a defined flow field and prescribed time step, the MMOC algorithm begins by backtracking along a velocity characteristic to the foot of the characteristic $\tilde{\mathbf{x}}_i$. The concentration at the foot of the characteristic $\tilde{C}(\tilde{\mathbf{x}}_i)$ is then approximated using an interpolation procedure. The grid point from which the particle backtracked, then assumes the interpolated concentration $\tilde{C}_i$, which is subsequently dispersed using a Galerkin FEM (Neuman, 1984; Healy and Russell, 1989; Yeh et al., 1993).

Eq. (7) can be expressed in Lagrangian form as:

$$\frac{\mathrm{d}C}{\mathrm{d}t} = \nabla\cdot(\theta\boldsymbol{D}\cdot\nabla C), \tag{14}$$

where:

$$\frac{\mathrm{d}C}{\mathrm{d}t} = \frac{\partial C}{\partial t} + \boldsymbol{v}\nabla\cdot C \tag{15}$$

represents the total derivative, which indicates the rate of change of C along velocity characteristics.

Single-step reverse particle tracking (Neuman, 1984) is used to backtrack along velocity characteristics. With this approach, a fictitious particle from grid point $\mathbf{x}_i$, is sent backward to the point $\tilde{\mathbf{x}}_i$, which is defined as:

$$\tilde{\mathbf{x}}_i = \mathbf{x}_i - \int_{t_k}^{t_{k+1}} \mathbf{v}_i \mathrm{d}t. \tag{16}$$

Eq. (16) infers that a particle leaving $\tilde{\mathbf{x}}_i$ at t_k will arrive at the grid point $\mathbf{x}_i$ at t_{k+1}. Velocities are assumed to be piece-wise linear, which is consistent with the approximation method used for the Darcy flux.

The solute concentration $\tilde{C}_i$ at $\tilde{\mathbf{x}}_i$, is approximated by interpolation, using:

$$\tilde{C}_i = \sum_{j=1}^{n_I} C_j(\mathbf{x}_j)\, N_j(\mathbf{x}_i), \tag{17}$$

where N_j is a shape function and n_I represents the number of nodes used in the interpolation. The grid point $\mathbf{x}_i$ then assumes $\tilde{C}_i$ as the advected concentration at time t_{k+1}. If $\tilde{\mathbf{x}}_i$ reaches across an inflow boundary, it is assigned the concentration at the boundary. At no-flow boundaries the particle is reflected back into the domain.

Once the advected concentration $\tilde{C}_i$ is determined at each node, the dispersive flux is approximated by solving Eq. (14) using a Galerkin finite-element method. A backward-difference time-stepping scheme is used along with mass lumping. The matrix-vector form can be expressed as:

$$[A_c]^{l+1}\{C_i\}^{l+1} = \{B_c\}^{l+1}. \tag{18}$$

The discretized form of the advective–dispersive equation is given in Appendix A. For 1-D simulations, a direct banded LUD solver is used to solve the matrix-vector equation. In 2-D, a biconjugate gradient squared iterative method with a Jacobi preconditioner from the NSPCG software package (Oppe et al., 1988) is applied.

The accuracy of the MMOC method in variably saturated media is a function of the technique used to backtrack a particle along a characteristic (Allen and Khosravani, 1990) and the interpolation method used to determine the advective concentration (Healy and Russell, 1989). When the velocity field is uniform, a simple one-step, Euler algorithm can be used to solve Eq. (16) accurately. In heterogeneous conditions, velocities can change rapidly over space and time. Backtracking accurately under these conditions can present difficulties. Various techniques have been suggested for tracking particles for complex velocity fields. The semi-analytical method described in Pollock (1988) is efficient and gives exact backtrack positions in 1-D heterogeneous systems. In brief, a particle travels from $\mathbf{x}_i$ to $\tilde{\mathbf{x}}_i$ moving across entire or partial elements in varying sub-intervals of time until the sum of the sub-intervals equals Δt. The sub-intervals of time are calculated analytically by knowing the nodal velocities and assuming piece-wise linearity. In 2-D, where velocities vary linearly from node to node in both directions, the semi-analytical method is not applicable. Under these conditions, either fourth-order Runge–Kutta methods (e.g., Baptista et al., 1984; Yeh et al., 1993) or a multiple-step

Euler method (Allen and Khosravani, 1990) must be applied.

For the multiple-step Euler method, N Euler steps of length Δt_s are taken, such that:

$$\tilde{\mathbf{x}}_i^N = \mathbf{x}_i^{N-1} = \boldsymbol{v}_i \Delta t_s, \tag{19}$$

where:

$$\Delta t = \sum_{s=1}^{N} \Delta t_s, \tag{20}$$

and for the multiple-step, fourth-order Runge–Kutta method, N equal sub-intervals of Δt_s are taken, as in:

$$\tilde{\mathbf{x}}_i^N = \mathbf{x}_i^{N-1} - \frac{1}{6}\left(\Delta x_i^1 + 2\Delta x_i^2 + 2\Delta x_i^3 + \Delta x_i^4\right), \tag{21}$$

where:

$$\begin{aligned} \Delta x_i^1 &= \left(\boldsymbol{v}_i \Delta t_s\right)_{x_i} \\ \Delta x_i^2 &= \left(\boldsymbol{v}_i \Delta t_s\right)_{x_i + \Delta x_i^1/2} \\ \Delta x_i^3 &= \left(\boldsymbol{v}_i \Delta t_s\right)_{x_i + \Delta x_i^2/2} \\ \Delta x_i^4 &= \left(\boldsymbol{v}_i \Delta t_s\right)_{x_i + \Delta x_i^3}. \end{aligned} \tag{22}$$

Interpolation of the concentration at the foot of the characteristic is commonly performed using a linear method. However, near steep concentration fronts, linear interpolation will introduce numerical dispersion in the solution (Cheng et al., 1984; Healy and Russell, 1989). Second-order accurate quadratic interpolation will reduce numerical dispersion, but it can produce oscillations in the solution (Cheng et al., 1984). For 1-D transport problems, Healy and Russell (1989) have shown that a combination of quadratic and linear interpolation can produce oscillation-free solutions with reduced dispersion. In their method, quadratic interpolation is applied first, a criteria is then used to test for an oscillation, and, if an oscillation exists, the concentration is recalculated using linear interpolation. Linear, quadratic, and quadratic–linear interpolation methods were incorporated into the MMOC transport model, as well as the multi-step Euler and fourth-order Runge–Kutta backtracking techniques. An analysis of the backtracking and interpolation methods is conducted in Section 4 to determine the most appropriate methods for 2-D transient, unsaturated, heterogeneous conditions.

4. Test examples

Test examples were designed to demonstrate the performance of the flow, Darcy flux, and transport algorithms in 1-D and 2-D water-unsaturated systems. Test problems also are used to investigate the performance of backtracking and interpolation techniques used in the application of the MMOC method.

4.1. 1-D flow example

To evaluate the performance of the flow model, simulations were conducted using the 1-D numerical experiment of Celia and Bouloutas (1990). The test represents the infiltration of water into a dry porous media. The porous media hydraulic properties for the test are defined by Eqs. (3)–(5) where $\theta_{ir} = 0.102$, $\theta_s = 0.381$, $\alpha = 0.0335$ cm^{-1}, $n = 2$, and $K_s = 0.00922$ cm s^{-1}. The initial condition is $\psi(z,0) = -1000$ cm. The boundary conditions are $\psi(0,t) = -75$ cm (top) and $\psi(100,t) = -1000$ cm (bottom). Two grid sizes ($\Delta z = 0.5$ and 2.5 cm) were used along with a fixed time step ($\Delta t = 600$ s). The simulations evolved for 24 h. The solutions were compared to a dense grid solution ($\Delta z = 0.125$). The results shown in Fig. 1 agree with the results shown in Figure 6a of Celia and Bouloutas (1990). The solutions are oscillation-free and converge to the dense grid solution. The relative mass balance error for these simulations was on the order of 10^{-4}%.

4.2. 2-D flow example: constant infiltration

To test the application of the flow model in 2-D heterogeneous conditions, a simulation was conducted using Test Problem 1 of Kirkland et al. (1992). The unsaturated test region, shown in Fig. 2, is 500 cm wide by 300 cm deep and is divided upto nine alternating blocks of clay and sand. The hydraulic parameters of the sand are given as $\theta_{ir} = 0.0286$, $\theta_s = 0.3658$, $\alpha = 0.0280$ cm^{-1}, $n = 2.239$, and $K_s = 541.0$ cm day^{-1}. The clay hydraulic parameters are $\theta_{ir} = 0.1060$, $\theta_s = 0.4686$, $\alpha = 0.0104$ cm^{-1}, $n = 1.3954$, and $K_s = 13.1$ cm day^{-1}. A constant flux of 5 cm day^{-1} was applied to the top center 100 cm of the domain and a no-flux boundary condition was applied to all other boundaries. The initial pressure head was defined as $-50{,}000$ cm. The simulation evolved for 12.5 days using a constant time step ($\Delta t = 4000$ s) and the grid spacing was $\Delta z = \Delta x = 5$ cm. Given that the domain is symmetric about the vertical center, only the right half of the domain was simulated.

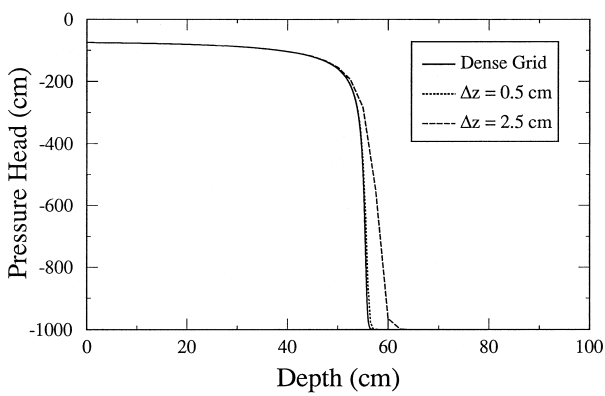

Fig. 1. Pressure head profile as a function of depth after 24 h and grid size for the Celia and Bouloutas (1990) test case.

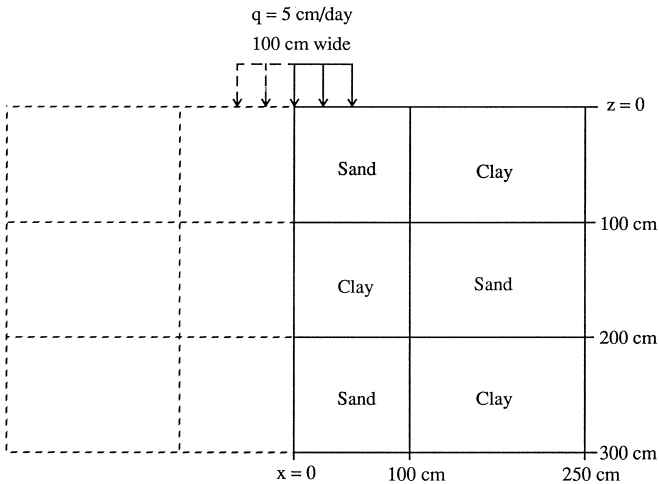

Fig. 2. Unsaturated domain for comparison with the Kirkland et al. (1992) test case. Zero-flux boundary conditions are applied except as noted. All dimensions are in centimeters. The figure is modified from Figure 1 in Kirkland et al. (1992). Note that only the right half of the domain, designated with solid lines, is simulated here.

The pressure head contours produced by the model described here, which are not shown, were similar to those presented in Figure 6 of Kirkland et al. (1992). The relative mass balance error for the simulation was on the order of 10^{-4}%. Shown in Fig. 3 is the horizontal flux profile calculated at $z = 95$ cm. The horizontal flux profile is in good agreement with the finer grid ($\Delta x = 2.5$ cm) finite-difference flux solution given in Figure 4 of Kirkland et al. (1992). However, an oscillation in the vertical flux solution occurs at one of the sand-clay boundaries, as shown in Fig. 4 for $x = 5$ cm. The oscillation arises because of the sharp changes in pressure and in hydraulic conductivity

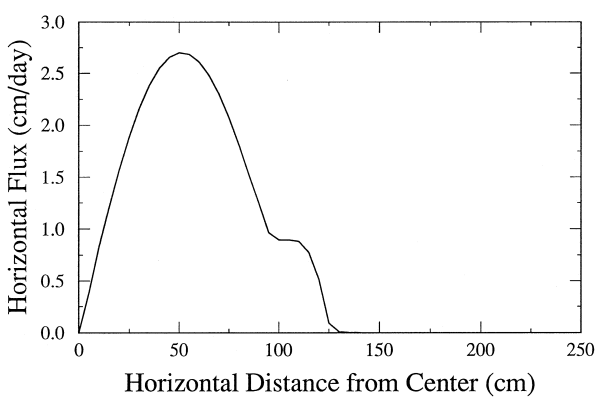

Fig. 3. Horizontal flux along the $z = 95$ cm position measured from the center of the domain after 12.5 days for the Kirkland et al. (1992) test case.

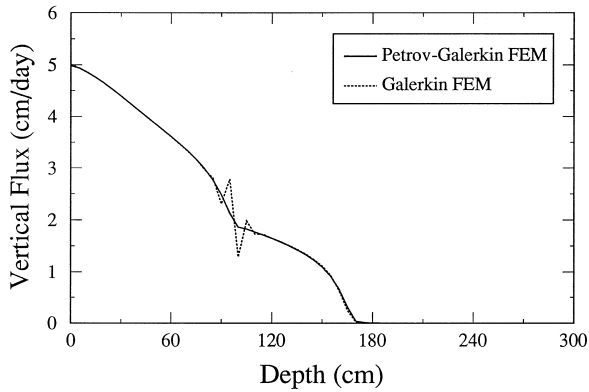

Fig. 4. Vertical flux along the $x = 5$ cm position after 12.5 days for the Kirkland et al. (1992) test case.

found at the sand clay boundary. The Galerkin finite-element method used to approximate the Darcy flux forces local flux conservation at the nodes, which produces a poorly-behaved solution when sharp changes in conductivities and pressures occur between nodes. The oscillations can be eliminated by using an upstream-weighted residual method such as a Petrov–Galerkin approximation (Westerink and Shea, 1989). The solution obtained with the Petrov–Galerkin approximation is shown to be oscillation-free in Fig. 4 and is in good agreement with the finer grid solution from Figure 5 of Kirkland et al. (1992).

4.3. 2-D flow example: transient infiltration

A similar experiment to Test 1 of Kirkland et al. (1992) was performed, where a transient rather than a constant flux was applied to the surface. The purpose of this experiment was to test the ability of the hysteresis algorithm to close scanning loops and

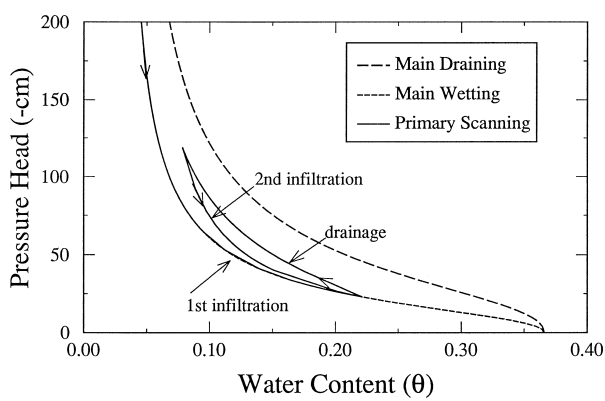

Fig. 5. Main wetting and drying pressure head–water content curves for the Berino loamy sand along with the primary scanning curves for the node at (5, 5 cm) resulting from the transient infiltration experiment.

maintain good mass balance. The transient flux alternated between $q_0 = 20$ cm day^{-1} (1 day), $q_0 = 0$ (6 days), and $q_0 = 20$ cm day^{-1} (1 day). The pressure head and water content were monitored throughout the simulation at a grid point positioned in the sand at ($x = 5$, $z = 5$ cm). Fig. 5 shows the main wetting and drying curves for this point, along with the primary scanning pressure head–water content curves resulting from the simulation. As expected with the method of Parker and Lenhard (1987), the scanning curves are closed, which resulted in good mass balance accuracy. A relative mass balance error on the order of 10^{-4}% was maintained throughout the experiment.

4.4. 2-D transport example: backtracking tests

In the following tests, numerical experiments are conducted to determine the accuracy and efficiency of backtracking techniques for 2-D transient, unsaturated, heterogeneous conditions. Multiple-step Euler and Runge–Kutta backtracking algorithms are considered. A 2-D grid (Fig. 6) consisting of 1-cm square elements was used to examine the two backtracking algorithms. The velocities in the domain represent severe changes in velocity that might be encountered in heterogeneous conditions. Nodes 7–9 in Fig. 6 are assigned a velocity of 1×10^{-1} cm s^{-1} while all other nodes are assigned a velocity of 1×10^{-3} cm s^{-1}. A time step size ($\Delta t = 500$ s) was chosen such that a particle backtracking from node $\mathbf{x}_i$ would cross the discontinuity at the element boundary and reach $\tilde{\mathbf{x}}_i$ in Δt (Fig. 6). The velocities in the x-direction were set equal to the velocities in the z-direction. Since $v_x = v_z$, and, by assuming that the velocity varies linearly between nodes, an analytical solution could be obtained for comparison purposes. For analysis of the Euler and fourth-order Runge–Kutta algorithms, N was chosen such that the number of function evaluations were equal. Given that the fourth-order Runge–Kutta method requires about four times the amount of function evaluations as that of the Euler

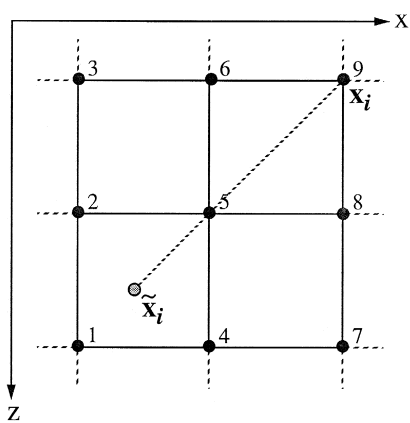

Fig. 6. Two-dimensional grid representing the boundary between two types of porous media. The velocities at nodes 1–6 are $v_x = v_z = 10^{-3}$ cm s^{-1} and the velocities at nodes 7–9 are $v_x = v_z = 10^{-1}$ cm s^{-1}. The point $\tilde{\mathbf{x}}_i$ represents the backtrack position from the node $\tilde{\mathbf{x}}_i$.

Table 1
Error Analysis

Method*	Error**
Multiple-Step Euler	
Δt_{240}	2.95×10^{-1}
Δt_{700}	9.82×10^{-2}
Δt_{2000}	$3.42\times10-2$
Fourth-Order Runge-Kutta	
Δt_{60}	4.27×10^{-3}
Δt_{175}	3.97×10^{-4}
Δt_{500}	2.64×10^{-5}

*Δt_s is the subinterval of the time step Δt, where s is the number of subintervals.
** Relative error (%) between the analytical backtrack result and the backtrack position approximated by the multi-step Euler and the multi-step fourth-order Runge-Kutta methods.

method, an $N = 240$ for the Euler method corresponds to an $N = 60$ for the fourth-order Runge–Kutta method.

The results of the test are shown in Table 1. The error shown in the table is the relative error (%) between the analytical solution and the values determined by the two multi-step techniques. Since the Euler method is only first-order accurate, it gives poor approximations of the backtracked position. Even with an $N = 2000$, the Euler method does not reach the lowest degree of accuracy achieved by the fourth-order Runge–Kutta method (Δt_{60}). Therefore, it can be concluded that the multi-step fourth-order Runge–Kutta method is more accurate and more efficient than the multi-step Euler method. Similar results have been obtained in one-dimensional tests of the two methods (Mitchell and Mayer, 1994). In regions of relatively high concentrations (in or near a solute plume), the multi-step fourth-order Runge–Kutta method should be used to backtrack. In regions outside the vicinity of a plume, an Euler method can be applied to improve overall computational efficiency.

4.5. 1-D transport example: interpolation test

For the 1-D case, the transport model was tested with each interpolation method against the analytical solution of Ogata and Banks (1961) for nonreactive solute transport. A 60-cm 1-D domain was chosen with a steady-state velocity field having a magnitude of 5×10^{-4} cm s^{-1}. The domain was discretized into 120 elements ($\Delta z = 0.5$ cm). Initially, the concentration was set to zero ($C(z,t<0)=0$). A Dirichlet boundary condition was applied at the left boundary ($C(0,t)=1$) and a no-flux condition was fixed at the right boundary.

Interpolation accuracy is controlled by the Cr number in a steady-state flow field. If Δz, Δt, and v are chosen such that Cr is an integer value, particles backtrack from node to node. Under these circumstances, there is no error due to interpolation. To demonstrate this case, a time step of 2000 s was chosen, which corresponds to Cr = 2. The result after 40 time steps is shown in Fig. 7. The solution using linear interpolation

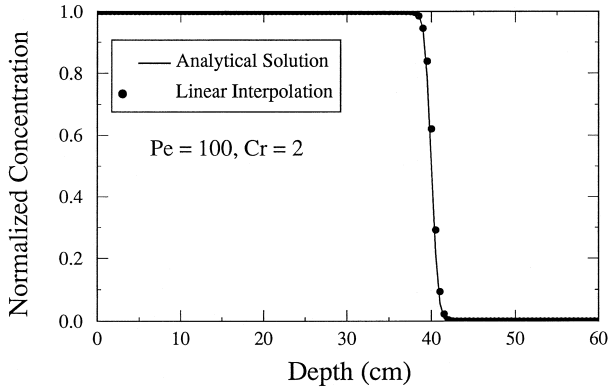

Fig. 7. Normalized concentration profile with depth after 50 times steps ($\Delta t = 2000$ s). Displayed are the analytic solution and numerical solution using linear interpolation for the case where Cr = 2 and Pe = 100.

matches the analytical solution very well. Identical results were achieved from all three interpolation methods. A numerical solution produced by either a Galerkin or Petrov–Galerkin finite-element method in this case would have oscillations because the methods are limited to $Cr \leq 1$ (Westerink and Shea, 1989).

Interpolation error arises when the foot of the characteristic lies between nodes, which occurs when the Cr number has non-integer values. The maximum error occurs when the foot of the characteristic lies in the center of an element, corresponding to a Cr number that is a factor of 0.5 (0.5, 1.5, 2.5, etc.). To test the performance of the three interpolation schemes for this extreme case, a time step of 1500 s was chosen, which corresponds to Cr = 1.5. The dispersivity was adjusted to produce test cases with Pe = 10 and Pe = 100. Simulations were carried out for 50 time steps.

Fig. 8 shows the analytical solution and the numerical solutions from the linear and quadratic interpolation methods, respectively, for the case when Pe = 10. The solution

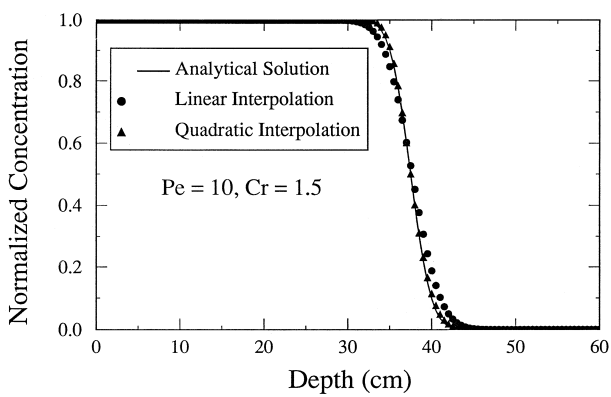

Fig. 8. Normalized concentration profile with depth after 50 times steps ($\Delta t = 1500$ s). Displayed are the analytic solution and numerical solutions using linear and quadratic interpolation for the case where Cr = 1.5 and Pe = 10.

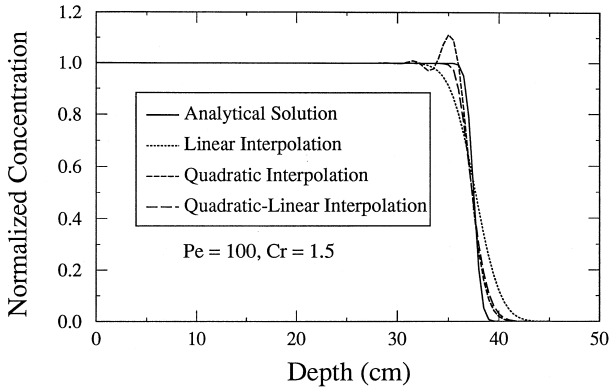

Fig. 9. Normalized concentration profiles with depth after 50 times steps ($\Delta t = 1500$ s). Displayed are the analytic solution and numerical solutions using linear, quadratic, and quadratic–linear interpolation for the case where Cr = 1.5 and Pe = 100.

resulting from the quadratic interpolation is in close agreement with the analytic solution and is free of oscillations in this case. The quadratic–linear method produced the same result (not shown) as the quadratic interpolation method. Numerical dispersion appears in the solution when applying linear interpolation. The dispersion due to linear interpolation increases as Pe $\rightarrow \infty$, as is demonstrated in Fig. 9 for the case where Pe = 100. The numerical solution generated for Pe = 100 with quadratic interpolation is shown in Fig. 9 with the corresponding analytical solution. The results shown in Fig. 9 demonstrate that oscillations will occur when applying the quadratic interpolation at non-integer Cr and high Pe. The oscillations tend to increase with the Pe number. The quadratic–linear method eliminates the oscillations, as shown in Fig. 9, while producing slight numerical dispersion. A comparison of the profiles given in Fig. 9 reveals that the numerical dispersion produced with the quadratic–linear method is smaller than that produced by the linear method. From the results of this analysis, it is apparent that the quadratic–lin-

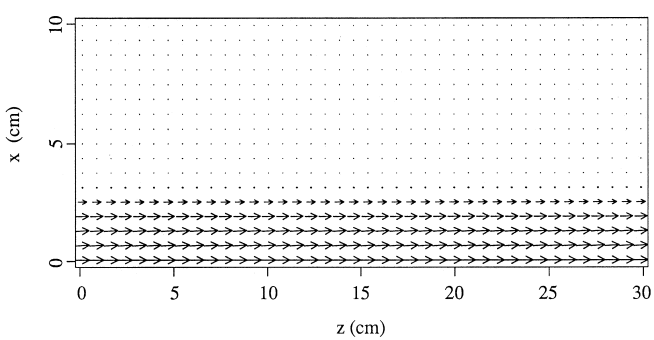

Fig. 10. Two-dimensional steady-state flow field representing a preferential flow path in a dry media. The largest velocity vector has a magnitude of 2.5×10^{-3} cm s^{-1} and v_z is represented as approximately $10 \times v_x$.

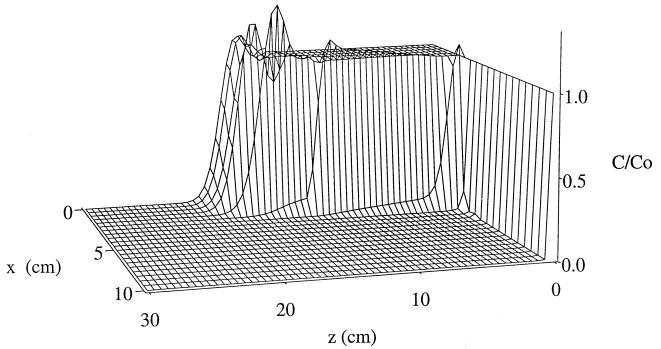

Fig. 11. Normalized concentration (C/C_0) surface plot resulting after 5000 s using quadratic interpolation.

ear technique is superior to both the linear and quadratic schemes for interpolating concentrations.

4.6. 2-D transport example

To test the MMOC model in a more complex flow field, the model was applied to simulate the transport of a nonreactive solute in a preferential flow path within a dry vadose zone. The velocity distribution for the problem is shown in Fig. 10. The dispersivities were chosen to be small $(\lambda_L = \lambda_T = 10^{-5}$ cm) to produce a highly advective problem. The flow field in this problem presents a severe test for the transport component of the model, due to the wide range of Peclet numbers $(0 < Pe_x < 1$ and $0 < Pe_z < 126)$ and Courant numbers $(0 < Cr_x < 0.1$ and $0 < Cr_z < 1.54)$. The simulations were conducted with Dirichlet boundary conditions along the $z = 0$ cm boundary $(C_0 = 1$ for $0 \le x \le 10$ cm), and the $z = 30$ cm boundary $(C_0 = 0$ for $0 \le x \le 10$ cm) and no-flux boundary conditions on other boundaries. The domain contained 1281 nodes $(\Delta x = \Delta z = 0.5$ cm). Simulations were run for a total time of 7500 s using a $\Delta t = 300$ s.

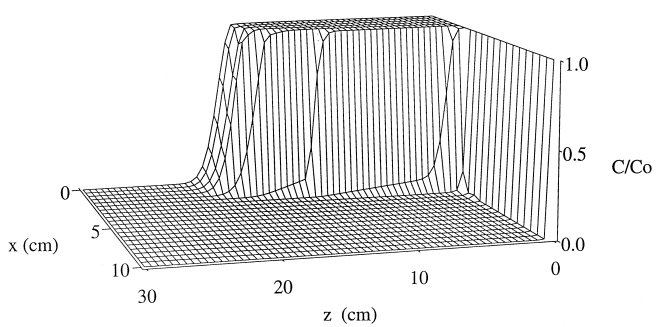

Fig. 12. Normalized concentration (C/C_0) surface plot resulting after 5000 s using quadratic–linear interpolation.

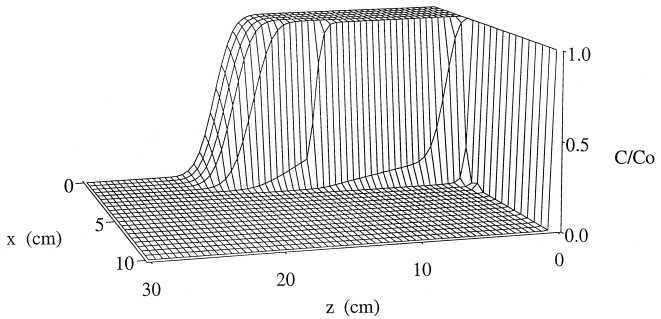

Fig. 13. Normalized concentration (C/C_0) surface plot resulting after 5000 s using linear interpolation.

The concentration distribution shown in Fig. 11 is a result of applying quadratic interpolation. The plot illustrates the oscillations that will occur when the Pe numbers are high and when only quadratic interpolation is applied. Fig. 12 shows that the oscillations can be eliminated when the quadratic–linear interpolation method is employed. Note also, that the profile in Fig. 12 retains the same steep advective characteristic displayed in Fig. 11. The results from using linear interpolation in the model are shown in Fig. 13. As expected, the solution is numerically dispersed, when compared to the other two interpolation methods, with the dispersion being greatest along the direction of flow (z-axis).

5. Conclusions

A 2-D numerical model was developed for simulating transient, hysteretic flow and nonreactive solute transport in unsaturated porous media. The uniqueness of the model is that it employs a combination of numerical formulations that previously have been demonstrated to accurately solve Richards', the Darcy flux, and the advection–dispersion equations. The formulations were applied, and in some instances, enhanced to perform accurately and efficiently in 2-D heterogeneous, unsaturated conditions.

The mixed form of Richards' equation and the numerical formulation described by Celia and Bouloutas (1990) was used to approximate the flow equation. The flow component of the model was subjected to the infiltration test of Celia and Bouloutas (1990) and was shown to produce accurate solutions with excellent mass balance in 1-D and agree with the results published in Celia and Bouloutas (1990). The flow model also reproduced, with good mass balance accuracy, the results of a 2-D numerical experiment of Kirkland et al. (1992). This experiment simulated infiltration of water into a 2-D domain consisting of initially, very dry alternating blocks of sand and clay. A transient experiment was also performed in the 2-D domain of Kirkland et al. (1992) and it was demonstrated that the hysteresis algorithm of Parker and Lenhard (1987) produced closed hysteretic scanning curves and conserved mass.

The finite-element scheme described by Srivastava and Brusseau (1995), which is a modification of the finite-element method described by Yeh (1981), was used to

determine the Darcy flux field. The finite-element method produced oscillations in the vertical flux solution at boundaries where a high contrast in hydraulic properties resulted in a severe pressure discontinuity during infiltration. However, by applying a Petrov–Galerkin finite-element technique to the flux equations, an oscillation-free and accurate solution was attained.

A modified method of characteristics technique was used to approximate solute transport. A variety of backtracking and interpolation methods were examined. It was determined that a fourth-order Runge–Kutta method is superior to other algorithms for backtracking along characteristics in 2-D heterogeneous porous media. It was also shown that a quadratic–linear interpolation technique outlined by Healy and Russell (1989) can be extended to two dimensions and is superior to both linear and quadratic interpolation. When these techniques are employed, the MMOC model proved to be effective in 2-D, unsaturated domains having a range of Pe and Cr numbers.

Appendix A. Discretized equations

The discretized form of Richards' equation is given as:

$$\int\int_D \left[\left(-\frac{N_k}{\Delta t}\frac{\mathrm{d}\theta}{\mathrm{d}\psi}\bigg|^{l+1,m} \right)\hat{\psi}_i^{\,l+1,m+1} + \left(\frac{\partial N_k}{\partial x} K_x^{l+1,m} \right)\frac{\partial \hat{\psi}_i^{\,l+1,m+1}}{\partial x} + \left(\frac{\partial N_k}{\partial z} \times K_z^{l+1,m} \right)\frac{\partial \hat{\psi}_i^{\,l+1,m+1}}{\partial z} \right] \mathrm{d}x\,\mathrm{d}z = \int\int_D \left[-\left(\frac{N_k}{\Delta t}\theta^{l+1,m} \right) + \left(\frac{N_k}{\Delta t}\theta^{l} \right) - \left(\frac{N_k}{\Delta t}\frac{\mathrm{d}\theta}{\mathrm{d}\psi}\bigg|^{l+1,m} \hat{\psi}_i^{\,l+1,m} \right) - \left(\frac{\partial N_k}{\partial z} K_z^{l+1,m} \right) \right] \mathrm{d}x\,\mathrm{d}z,$$

where Δt is the time step size, and in the Galerkin finite-element approximation, $\hat{\psi}_i$ designates a trial function:

$$\hat{\psi}_i = \sum_{j=1}^{n} N_j \psi_j,$$

where N_k is the linear shape function, which is equivalent to the weighting function.

The discretized form for the x-component of the Darcy flux is given as:

$$\int\int_D \left(N_k \hat{q}_x^{\,l+1} \right)\mathrm{d}x\,\mathrm{d}z = \int\int_D \left[-\left(N_k K_x^{l+1,m} \right)\frac{\partial N_k}{\partial x}\psi_i^{\,l+1} \right]\mathrm{d}x\,\mathrm{d}z,$$

and the z-component of the Darcy flux is expressed as:

$$\int\int_D \left(N_k \hat{q}_z^{\,l+1} \right)\mathrm{d}x\,\mathrm{d}z = \int\int_D \left[-\left(N_k K_z^{l+1,m} \right)\frac{\partial N_k}{\partial z}\psi_i^{\,l+1} + \left(N_k K_z \right) \right]\mathrm{d}x\,\mathrm{d}z,$$

where:

$$\hat{q}_i = \sum_{j=1}^{n} N_j q_j.$$

The discretized form of Eq. (14) is given as:

$$\int\int_D \left[\left(\frac{N_k}{\Delta t} \theta^{l+1} \right) \hat{C}_i^{l+1} + \left(\frac{\partial N_k}{\partial x} D_{xx}^{l+1} \right) \frac{\partial \hat{C}_i^{l+1}}{\partial x} + \left(\frac{\partial N_k}{\partial x} D_{xz}^{l+1} \right) \frac{\partial \hat{C}_i^{l+1}}{\partial z} + \left(\frac{\partial N_k}{\partial z} \times D_{zx}^{l+1} \right) \frac{\partial \hat{C}_i^{l+1}}{\partial x} + \left(\frac{\partial N_k}{\partial z} D_{zz}^{l+1} \right) \frac{\partial \hat{C}_i^{l+1}}{\partial z} - (N_k q_s) \hat{C}_i^{l+1} \right] \mathrm{d}x\, \mathrm{d}z$$

$$= \int\int_D \left[\left(\frac{N_k}{\Delta t} \theta^{l+1,m} \right) \hat{C}_i^{l} - (N_k q_s) C_0 \right] \mathrm{d}x\, \mathrm{d}z,$$

where:

$$\hat{C}_i = \sum_{j=1}^{n} N_j \tilde{C}_j,$$

and q_s and C_0 are the prescribed surface flux and concentration, respectively.

References

Allen, M.B., Khosravani, A., 1990. An Eulerian–Lagrangian method for finite-element collocation using the modified method of characteristics. In: Gambolati, G., Rinaldo, A. et al. (Eds.), Proc. Eighth Int. Conf. Comput. Meth. in Water Resources, Computational Methods in Surface Hydrology. Springger, Southampton, UK, pp. 375–380.

Allen, M.B., Murphy, C.L., 1986. A finite element collocation method for variable saturated flow in two space dimensions. Water Resources Res. 22, 1537–1542.

Baptista, A.M., Adams, E.E., Stolzenbach, K.D., 1984. The 2-D, unsteady, transport equation solved by the combined use of the finite element method and the method of characteristics. In: Proc. 5th Int. Conf. Finite Elements in Water Res. Springer, Berlin, Germany, pp. 353–362.

Bear, J., 1979. Hydraulics of Groundwater, McGraw-Hill, New York.

Binning, P., Celia, M.A., 1996. A finite volume Eulerian–Lagrangian localized adjoint method for solution of the contaminant transport equations in two-dimensional multiphase flow systems. Water Resources Res. 32 (1), 103–114.

Bresler, E., Dagan, G., 1981. Convective and pore scale dispersive solute transport in unsaturated heterogeneous fields. Water Resources Res. 17 (6), 1683–1693.

Cantekin, M.E., Westerink, J.J., 1990. Non-diffusive N+2 degree Petrov–Galerkin methods for two-dimensional transient transport computations. Int. J. Numerical Meth. Fluids 30, 394–418.

Celia, M.A., Bouloutas, E.T., 1990. A general mass-conservative numerical solution for the unsaturated flow equation. Water Resources Res. 26 (7), 1483–1496.

Celia, M.A., Ahuja, L.R., Pinder, G.F., 1987. Orthogonal collocation and alternating-direction procedures for unsaturated flow problems. Adv. Water Resources 10, 178–187.

Cheng, R.T., Casulli, V., Milford, S.N., 1984. Eulerian–Lagrangian solution of the convective-dispersion equation in natural coordinates. Water Resources Res. 20 (7), 944–952.

Chiang, C.Y., Wheeler, M.F., Bedient, P.B., 1989. A modified method of characteristics technique and mixed finite elements method for simulation of groundwater solute transport. Water Resources Res. 25 (7), 1541–1549.

Gee, G.W., Kincaid, C.T., Lenhard, R.J., Simmons, C.S., 1991. Recent studies of flow and transport in the vadose zone. Rev. Geophysics Supplement, 227–235.

Healy, R.W., Russell, T.F., 1989. Efficient implementation of the modified method of characteristics in finite-difference models of solute transport. In: Proc. NWWA Conf. on Solving Ground Water Problems with Models. National Water Well Association, Columbus, OH, pp. 483–492.

Jaynes, D.B., 1984. Comparison of soil–water hysteresis models. J. Hydrology 75, 287–299.

Jury, W.A., 1982. Simulation of solute transport using a transfer function model. Water Resources Res. 18, 363–368.

Kirkland, M.R., Hills, R.G., Wierenga, P.J., 1992. Algorithms for solving Richards' equation for variably saturated soils. Water Resources Res. 28 (8), 2049–2058.

Kool, J.B., Parker, J.C., 1987. Development and evaluation of closed-form expressions for hysteretic soil hydraulic properties. Water Resources Res. 23 (1), 105–114.

Lenhard, R.J., Parker, J.C., 1987. A model for hysteretic constitutive relations governing multiphase flow: 2. Permeability–saturation relations. Water Resources Res. 23 (12), 2197–2206.

Lenhard, R.J., Parker, J.C., Kaluarachchi, J.J., 1991. Comparing simulated and experimental hysteretic two-phase transient fluid flow phenomena. Water Resources Res. 27 (8), 2113–2124.

Millington, R.J., Quirk, J.M., 1961. Permeability of porous solids. Trans. Faraday Soc. 57, 1200–1207.

Mitchell, R.J., Mayer, A.S., 1994. A modified method of characteristics technique for simulating contaminant transport in variably-saturated porous media. In: Peters, A. et al. (Ed.), Computational Methods in Water Resources X. Kluwer Academic Publishers, Dordrecht, The Netherlands, pp. 505–512.

Mualem, Y., 1976. A new model for predicting the hydraulic conductivity of unsaturated porous media. Water Resources Res. 12 (3), 513–522.

Neuman, S.P., 1984. Adaptive Eulerian–Lagrangian finite element method for advection–dispersion. Int. J. Numerical Meth. Eng. 20, 321–337.

Nielsen, D.R., van Genuchten, M.T., Biggar, J.W., 1986. Water flow and solute transport processes in the unsaturated zone. Water Resources Res. 22 (9), 89–108.

Noorishad, J., Tsang, C.F., Perrochet, P., Musy, A., 1992. A perspective on the numerical solution of convection-dominated transport problems: a price to pay for the easy way out. Water Resources Res. 28 (2), 551–561.

Ogata, A., Banks, R.B., 1961. A Solution of the Differential Equation of Longitudinal Dispersion in Porous Media. US Government Printing Office, Washington, DC.

Oppe, T.C., Joubet, W.D., Kincaid, D.R., 1988. NSPCG User's Guide: A Package for Solving Large Sparse Linear Systems by Various Iterative Methods. Center for Numerical Analysis, The University of Texas at Austin.

Parker, J.C., Lenhard, R.J., 1987. A model for hysteretic constitutive relations governing multiphase flow: 1. Saturation–pressure relations. Water Resources Res. 23 (12), 2187–2196.

Pollock, D.W., 1988. Semianalytical computation of path lines for finite-difference models. Ground Water 26 (6), 743–750.

Russo, D., Jury, W.A., Butters, G.L., 1989. Numerical analysis of solute transport during transient irrigation: 1. The effect of hysteresis and profile heterogeneity. Water Resources Res. 25 (10), 2109–2118.

Scott, P.S., Farquhar, G.J., Kouwen, N., 1983. Hysteretic effects on net infiltration, advances in infiltration. Am. Soc. Agric. Eng., Publ. 11-83, pp. 163–170, Chicago, IL.

Srivastava, R., Brusseau, M.L., 1995. Darcy velocity computations in the finite element method for multidimensional randomly heterogeneous porous media. Adv. Water Resources 18 (4), 191–201.

Sudicky, E.A., Huyakorn, P.S., 1991. Contaminant migration in imperfectly known heterogeneous groundwater systems. Rev. Geophysics Supplement, 240–253.

van Genuchten, M.T., 1980. A closed-form equation for predicting the hydraulic conductivity of unsaturated soils. Soil Sci. Soc. Am. J. 44, 892–898.

van Genuchten, M.T., 1991. Recent progress in modeling water flow and chemical transport in the unsaturated zone. In: Kienitz, G., Milly, P.C.D. et al. (Eds.), Hydrological Interactions Between Atmosphere, Soil and Vegetation. IAHS.

van Genuchten, M.T., Wierenga, P.J., 1976. Mass transfer studies in sorbing porous media: I. Analytical solutions. Soil Sci. Soc. Am. J. 40 (4), 473–480.

Westerink, J.J., Shea, D., 1989. Consistent higher degree Petrov–Galerkin methods for the solution of the transient convection–diffusion equation. Int. J. Numerical Meth. Eng. 28, 1077–1101.

Yeh, G.T., 1981. On the computation of Darcian velocity and mass balance in the finite element modeling of groundwater flow. Water Resources Res. 17 (5), 1529–1534.

Yeh, J.T.C., Srivastava, R., Guzman, A., Harter, T., 1993. A numerical model for water flow and chemical transport in variably saturated porous media. Ground Water 31 (4), 634–644.

Zhang, R., Huang, K., van Genuchten, M.T., 1993. An efficient Eulerian–Lagrangian method for solving solute transport problems in steady and transient flow fields. Water Resources Res. 29 (12), 4131–4138.